Effect of Dual Impeller-Sparger Geometry on the Hydrodynamics and Mass Transfer in Stirred Vessels

By *Daniel García-Cortés*, *Catherine Xuereb**, *Patricia Taillandier*, *Ulises Jáuregui-Haza*, and *Joël Bertrand*

The understanding of the effect of impeller-sparger configurations on gas dispersion and mass transfer is very important to improve the performance of gas/liquid contactor systems. The influence of the impeller positions, the upper turbine diameter, the sparger ring diameter and its location in regard to the lower impeller on the power consumption, the volumetric mass-transfer coefficient and the overall oxygen transfer efficiency were studied in a nonstandard curved bottomed reactor with an agitated system with dual disk style turbines. In the range of the gas flow rates studied, the most efficient impeller-sparger arrangement for the oxygen transfer is the impeller system with turbines of different diameters located at C = 0.25 and IC = 0.5, and with the sparger of smaller diameter than the lower impeller settled below the impeller. A new model to estimate the k_La with an average relative error of 8 %, which takes the reactor operation conditions and the influence of the impeller-sparger geometry into account, was also proposed.

1 Introduction

The gas/liquid contacting operations play an important role in several industrial processes. In the biotechnological industry, for example, oxygen transfer into the liquid phase determines, in many cases, the efficiency of the fermentation processes because of the low solubility of oxygen in aqueous media. The gas/liquid dispersion processes typically rely on the configuration of the disk style turbine in conjunction with a sparger positioned below the stirrer [1]. However, recently, attention has been paid to the influence of impeller-sparger configurations on gas dispersion by Birch and Ahmed [2] and on mass transfer by Rocha-Valadez *et al.* [3], due to the necessity to improve the performance of gas/liquid contactor systems. Nevertheless, the influence of the impeller-sparger configurations in multi-impeller systems is scarce even though these are often used industrially [4].

The gas/liquid dispersion process in flat bottomed reactors equipped with four symmetrically located wall baffles and with H > T[1)], the ring sparger smaller than the impeller diameter and dual turbine impellers has been extensively reported [5 8], but very little data concerning these aeration-agitation systems with H = T and the ring sparger larger than the impeller diameter are found in the literature [4,9]. On the other hand, few papers have been published on these systems with curved bottomed reactors [10] and with baffles located away from the wall.

The flows generated in vessels stirred with two turbine impellers of diameters D = T/3 and H = T were extensively studied by Rutherford *et al.* [11]. They stated that the flows depend strongly on the clearance of the lower impeller above the base of the vessel; the separation between the impellers and the submergence of the upper impeller below the top of the liquid column height. Besides, they observed three stable flow patterns called parallel, merging and diverging flow patterns.

The influence of clearance between the impellers on the hydrodynamics in different aerated-agitated standard systems has been studied by several authors [6,12]. Surprisingly, agitation systems with dual turbine impellers of different diameters have rarely been considered for gas dispersion.

The aim of this study is to evaluate the influence of the impeller positions, the upper turbine diameter, the sparger ring diameter and its location with respect to the lower impeller on the power consumption, the volumetric mass-transfer coefficient and the overall oxygen transfer efficiency in a nonstandard curved bottomed reactor with dual disk style turbines and a ring sparger.

2 Experimental

The experiments were performed in a nonstandard curved bottomed cylindrical tank with internal diameter T = 0.19 m and a bottom curvature radius of r = 0.19 m, equipped with various impeller-sparger configurations. Four baffles (0.1 T) were symmetrically mounted at 0.009 m away from the wall. The general layout of the aeration-agitation system and the dimensions in millimeters (mm) of the disk style turbines (DT) are shown in Fig. 1. The reactor was filled with water up to a liquid height of H = T and sparged with air.

Two spargers with ring diameters of $S_d = 0.65\ D_L$ and $S_d = 1.4\ D_L$, respectively were used. Both spargers had holes of 40 × 0.0006 m in diameter. Figs. 2 and 3, and Tabs. 1 and 2 detail the studied sparger locations and impeller configurations. The gas flow rates changed in the experiments in the range of 47 1835 L/h, which correspond to the range of flow numbers (Fl) 0.006 0.233, respectively.

The agitator shaft was extended to the bottom of the tank, fitting in a Teflon-made hub, in order to avoid excessive

[*] D. García-Cortés, U. Jáuregui-Haza, Centro de Química Farmacéutica. Ave. 200 y 21 Atabey, PB 16042, 11600 Habana, Cuba; Catherine Xuereb (e-mail: Catherine.Xuereb@ensiacet.fr), P. Taillandier, J. Bertrand, Laboratoire de Génie Chimique UMR CNRS 5503 – 5, rue Paulin Talabot – BP 1301 – 31106 Toulouse Cedex 1, France.

1) List of symbols at the end of the paper.

DOI: 10.1002/ceat.200401965

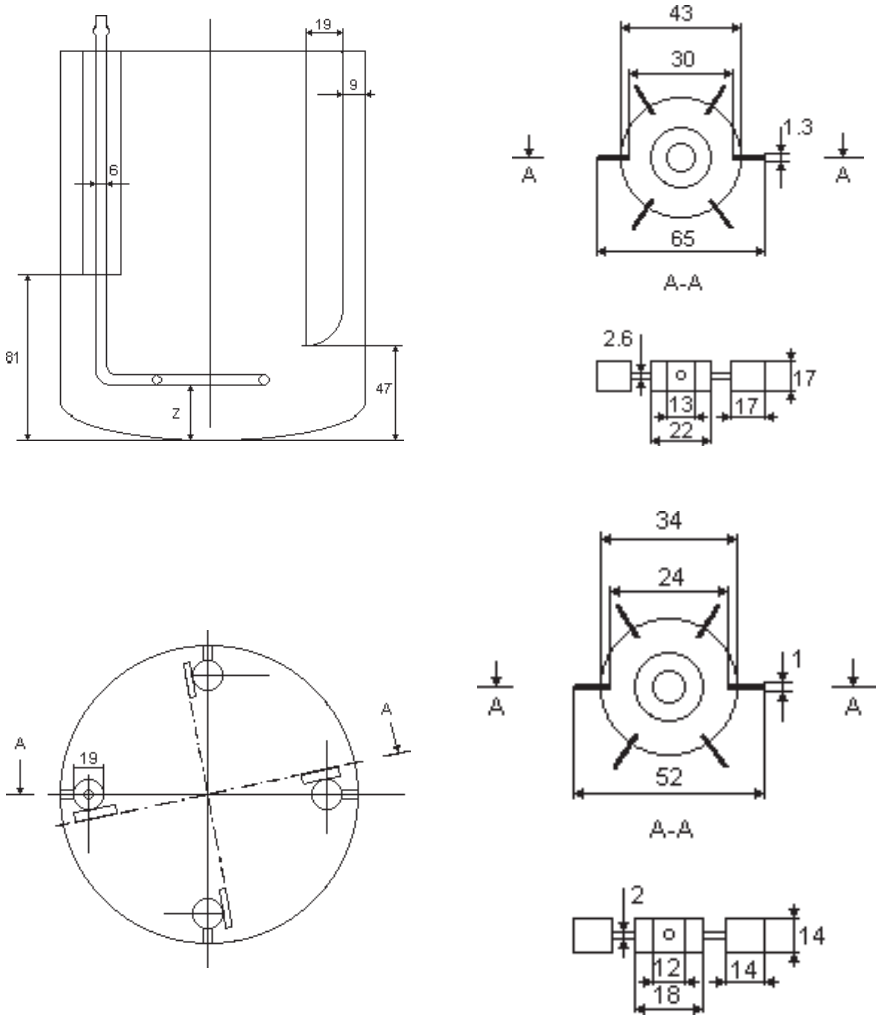

Figure 1. The vessel and impeller dimensions (mm).

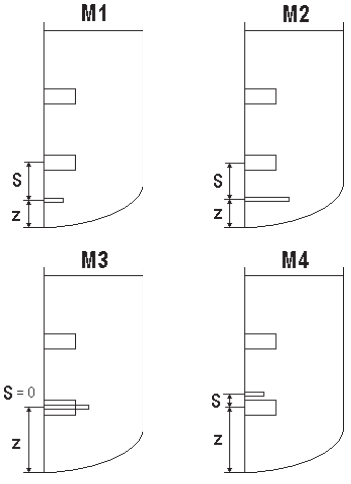

Figure 2. Example of sparger locations for the impeller configurations B.

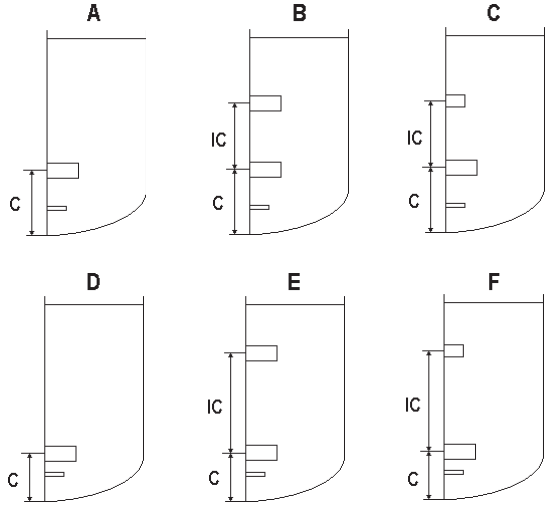

Figure 3. Example of impeller configurations for sparger position M1.

'wobbling' of the impeller. The rotational speed was 500 ± 1 rpm in all experiments which corresponds to a Reynolds number of 43800. The torque on the agitator shaft was measured by a torque-measuring coupler (Staiger and Mohilo) mounted in the agitator shaft. The experimental value of the torque was corrected for friction losses by measurements performed in the empty vessel and was then used to calculate the power consumption.

Table 1. Sparger locations.

Nomenclature	Ring sparger diameter, mm	Height from the reactor bottom, z/T	Clearance from the lower impeller to the sparger, S/T
M1	42	0.13	0.12 a C/T = 0.25 0.18 a C/T = 0.33
M2	92	0.13	0.12 a C/T = 0.25 0.18 a C/T = 0.33
M3	92	C/T	0
M4	42	0.32 a C/T = 0.25 0.40 a C/T = 0.33	–0.07*

* The negative value means that the sparger is located above the lower impeller.

Table 2. Impeller configurations.

Impeller configuration	Nomenclature	Upper impeller	Lower impeller	C	IC
DT65	A	–	DT65	0.33 T	–
DT65 + DT65	B	DT65	DT65	0.33 T	0.33 T
DT65 + DT52	C	DT52	DT65	0.33 T	0.33 T
DT65	D	–	DT65	0.25 T	–
DT65 + DT65	E	DT65	DT65	0.25 T	0.5 T
DT65 + DT52	F	DT52	DT65	0.25 T	0.5 T

The volumetric mass transfer coefficient k_La was measured using the startup dynamic method [13] with an oxygen probe positioned at the mid-height of the tank. The experimental data were nonlinearly regressed with a first-order model taking the response time of the probe τ into account, which was equal to 7.2 s, in order to calculate k_La. The choice of a first-order model for the gas phase is justified by the fact that such simplified models still preserve the relative order of merit of agitators, making them useful comparison purposes [14]. Furthermore, for low k_La values (< 0.06 s^{-1}), like those obtained in this study, the difference between first- and second-order (e.g., perfectly mixed or plug flow models) methods is negligible [15].

$$C_{Lm}(t) = \frac{C_{gi}}{m}\left(1 - \frac{k_L a\tau}{k_L a\tau - 1}\exp(-t/\tau) + \frac{1}{k_L a\tau - 1}\exp(-k_L at)\right) \quad (1)$$

The overall transfer efficiency (OTE) was calculated from the mass of oxygen transferred per hour divided by the power consumption [10].

$$OTE = k_L a\, C^* V_L/P_g \quad (2)$$

All the experiments were carried out at 30 °C. At this temperature the equilibrium concentration of oxygen in water is 7.63 mg O_2/mL [16].

3 Results and Discussion

3.1 Power Consumption and Hydrodynamics

The power input in the stirred tank reactor is the most important characteristic of the aerated-agitated systems because both mixing and mass-transfer properties are mainly dependent on them [17].

Hudkova *et al.* [6] pointed out that for a clearance between impellers larger than 0.67 T the power drawn by the dual impeller system approximates twice that of the single impeller system. However, this maximum value can be reached at an impeller spacing less than 0.67 T starting from a certain value of the agitation speed [18,19]. The interpretation given to this phenomenon is the decrease of the vertical amplitude of the volume of influence of each turbine increasing the agitation speed [19]. On the other hand, Kuboi and Nienow [9] measuring the power consumption of a dual impeller system in a standard reactor with C = IC = 1/3 T and H = T, obtained a power consumption of 1.5 times the power drawn by a single impeller system. That coincides approximately with the results of the measurements done by Rutherford *et al.* [11] (P_2/P_1 = 1.55) in a similar system to the previous one, in which they observed a merging flow pattern. Rutherford *et al.* [11] also reported that increasing the impeller clearance up to 0.5 T, this ratio increased up to 1.85. This value denotes that a certain interaction between impellers still exists, however, in their study they found that starting from IC = 0.385 T a parallel flow pattern is already observed.

The results of the ungassed power consumption measurement in the used reactor with different sparger-impeller arrangements are shown in Tab. 3.

As can be observed, the power drawn in configurations A and D are similar, which suggests that in the studied reactor geometry, characterized by a location of the baffles away from the wall and the bottom at 0.05 T and 0.25 T, respectively and by the curved bottom, the variation of the clearance of the impeller with regard to the bottom from 0.25 T to 0.33 T does not have a significant influence on the power consumption.

On the other hand, it is necessary to point out that in the configurations E and B, where IC is equal to 0.5 T and 0.33 T, respectively, the ratios P_2/P_1 of 1.46 and 1.24 were obtained (that means a reduction of P_2/P_1 of approximately 20 % with regard to that obtained by Rutherford *et al*. [11]), which denotes that in the reactor with nonstandard geometry there is a strong interaction between the impellers.

In the case of configurations C and F, where the upper impeller is 20 % proportionally smaller than the lower one, the power consumption is similar to that of the configurations with a single impeller (A and D). The probable cause of this behavior is the compensation of the increase of the power consumption due to the contribution of the upper impeller (1.1 W), with the decrease of the power drawn due to the interaction between both impellers. This hypothesis can be justified comparing the power consumption of the studied dual impeller agitation systems with different dimensions (C and F) with that of the dual impeller systems of equal dimensions (B and E). In the case of the configurations B and E, the decrease of the power consumption due to the interaction between the impellers, with regard to the maximum value of the power drawn by the system without interaction between the impellers (sum of the power drawn by each impeller when acting alone [20]) were 76 and 54 %, respectively. While, if the individual maximum contribution to the power consumption of the two impellers of different dimensions used in this study is compared, it could be observed that the contribution to the power consumption of the impeller of smaller dimensions would constitute around 30 % of the contribution of the greater impeller, which is, at once, smaller than the decrease of the power consumption obtained in the agitation systems with equal impellers (B and E) with regard to the possible maximum.

As was emphasized by Nienow *et al*. [20], visualization of the flow close to the agitator blades contributes to the understanding of gas dispersion processes. Gas filled cavities formed behind the blades and the shape and size of the cavities is one of the two parameters which control the power drawn by the agitator at a particular speed and aeration rate; the other one is the bulk flow. Both the cavity shape and the bulk flow phenomena are affected by the presence of multiple impellers on the shaft [6]. In turn, all these factors affect the gas/liquid mass transfer performance. Thus, consideration of all these factors has to be made for a proper assessment of any advantage accruing from changes of the impeller-sparger arrangement.

The variation of the power consumption ratio as a function of flow number, sparger clearance and ring sparger diameter is shown in Figs. 4 and 5. In general, it can be noticed that in all figures, the decrease of the power consumption in the gassed reactor is lower in the sparger arrangements with the largest ring diameter as has been reported before [4]. The difference between the power consumption curves in the single impeller configuration (C = 0.33 T) with spargers of different diameters (see Fig. 4a)), is based on the fact that with the sparger of small diameter, the large cavities behind the impellers are formed at low Fl, while with the larger sparger the large cavities are formed at higher Fl. For this reason, in the first case the decrease of the power consumption is more abrupt than in the second one. It is worth to point out that in the case in which the sparger is located level with the impeller, the air bubbles arrive at the impeller indirectly all the time [2].

In Fig. 4a) it can be observed that with the larger sparger positioned below the impeller (M2) the power consumption drop at very low air flow rates is more significant. This phenomenon happens because at these gas flows, bubbles of small diameter are obtained and the majority of them are dragged directly toward the impeller by the liquid streams. Increasing the air flow, the diameter of the bubbles grows and the direct to indirect loading transition occurs. This fact causes an increase of the power consumption until a maximum; a further increase of the Fl provokes a power consumption decrease due to the quantity of air that arrives indirectly at the impeller. The same phenomenon can be observed with other arrangements (e.g., M2D and M3D). Therefore, it can be concluded that the abrupt variations observed in the Figs. 4 and 5 are caused by the changes in the flow pattern of the air bubbles inside the reactor.

The behavior of the curve M3B is very similar to that of the curve M2A (see Fig. 4b)). In this case,

Table 3. Power consumption in the ungassed systems.

Impeller configuration	Po, W			
	Sparger arrangement			
	M1	M2	M3	M4
A	3.4 ± 0.1	3.2 ± 0.2	3.1 ± 0.3	–
B	4.20 ± 0.03	3.9 ± 0.4	4.0 ± 0.3	4.0 ± 0.4
C	3.4 ± 0.3	2.9 ± 0.3	3.0 ± 0.1	2.5 ± 0.1
D	3.5 ± 0.3	3.1 ± 0.1	3.1 ± 0.3	–
E	5.1 ± 0.3	5.1 ± 0.2	4.9 ± 0.2	4.8 ± 0.6
F	3.4 ± 0.3	3.6 ± 0.3	3.2 ± 0.1	3.3 ± 0.7

the relative position between the upper impeller and the sparger is similar to the relative position between the lower impeller and the sparger in the system M2A. In the arrangement M3B, at low Fl, the small bubbles arrive directly at the upper impeller ascending around the axis, although it is worth pointing out that in the arrangement M2A the range of Fl in which the bubbles arrive directly at the impeller is smaller. This is caused by the fact that at the same gas flow rate, the size of the bubbles in the arrangement M3B is smaller than in the arrangement M2A because in the first one, the sparger is located directly under the influence of fluid streams coming from the lower impeller.

The decrease of the power consumption at low Fl in dual impeller systems of different diameters and with the larger sparger positioned below the lower impeller (M2C) is less marked than in the arrangements M2A, M2B and M3B (see Fig. 4c)). This is probably caused by the fact that the power consumption drop provoked by the action of the bubbles on the lower impeller is compensated by the power drawn of the upper one. In the case of the arrangement M2B the larger diameter of the upper impeller in comparison with the arrangement M2C provokes a pumping capacity that is high enough to drag the bubbles and this way it cannot compensate for the fall of the power consumption of the lower impeller.

The shape of the curve corresponding to the arrangement of the single turbine with the sparger level to the impeller (M3D) corresponds to the fact that the bubbles arrive at the impeller indirectly and large cavities are formed at high Fl values (see Fig. 5a)). On the other hand, the power consumption of the dual turbine configuration with impellers of different diameters and the sparger level to the lower turbine show a remarkable variation (see Fig. 5c)). In this case, at low values of Fl, large cavities are observed in the upper impeller. While increasing the Fl, the bubble diameters increase, and the fluid streams cannot drag the dispersed bubbles towards the lower impeller. An increase in power consumption is noted. A further increase of the Fl causes a new fall in the power drawn until the large cavities are formed in the lower impeller and the upper one is flooded at high Fl.

3.2 Mass Transfer

Variation of the overall volumetric mass transfer coefficient in the systems with different sparger-impeller arrangements as a function of the flow number is shown in Figs. 6 and 7. The average relative error of k_La measurements was smaller than 1.5 %.

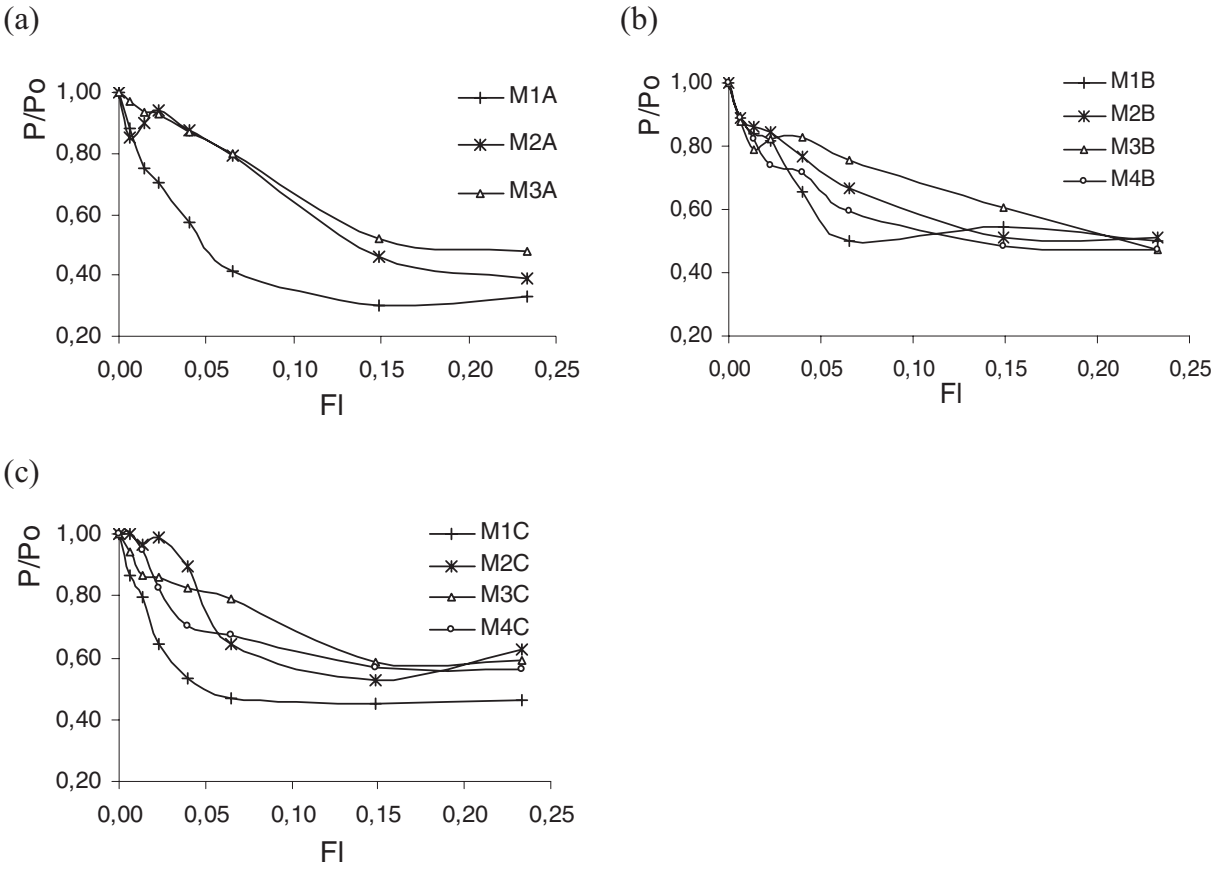

Figure 4. Power consumption in the reactor arrangement with C = 0.33 T. a) single impeller, b) dual impellers of the same diameter and c) dual impellers of different diameters.

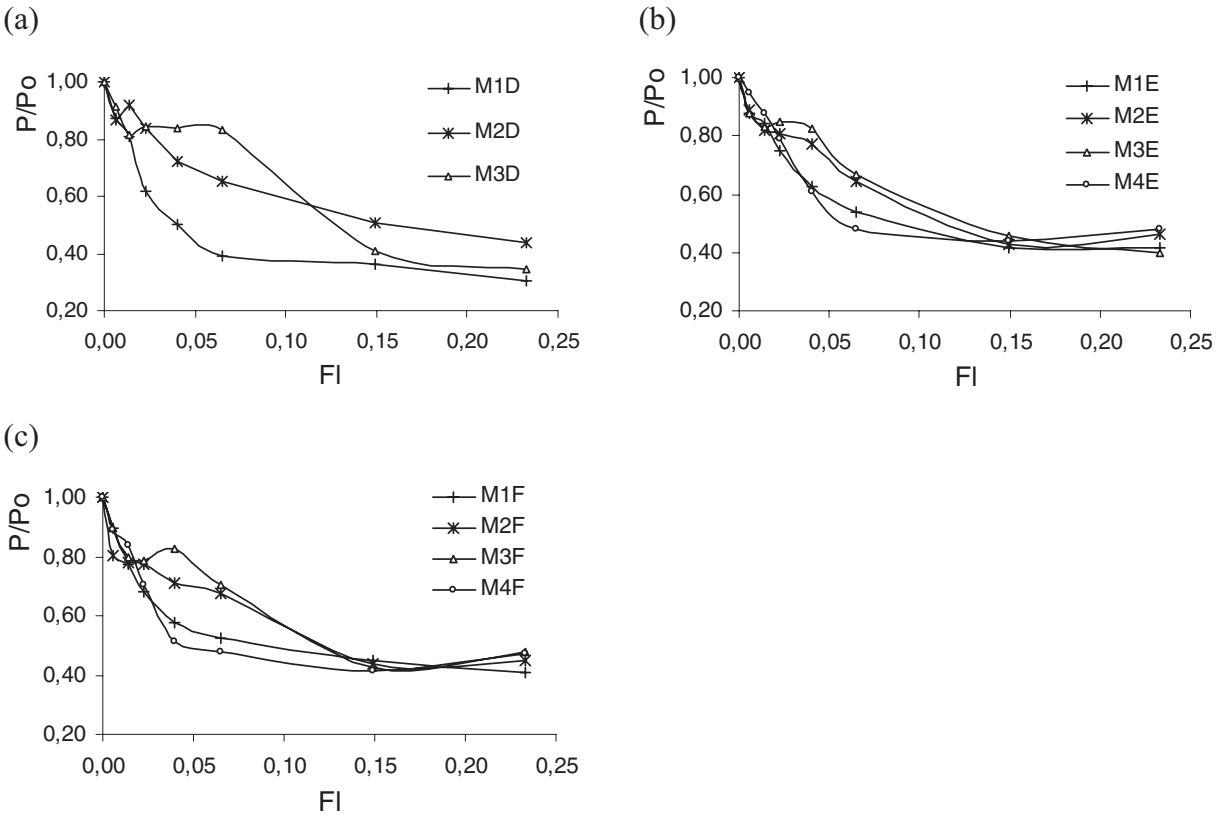

Figure 5. Power consumption in the reactor arrangement with C = 0.25 T. a) single impeller, b) dual impellers of the same diameter and c) dual impellers of different diameters.

Comparing the two previous figures, it can be observed that the increase of the k_La at small values of the Fl is bigger in the case of the agitation systems shown in the Fig. 7 where the impeller clearance between the impeller and the bottom is smaller and the clearance between the impellers is larger (cases b) and c)). It can be noticed that, at Fl values greater than 0.04, the best values of k_La are obtained with the spargers of larger ring diameter.

3.2.1 Volumetric Mass-Transfer Coefficient Modeling

The volumetric mass-transfer coefficient has been the subject of study by different authors, who have proposed some correlations for its estimation [10,21 29]. In this work, the predictive capacity of several k_La models obtained in coalescence systems was evaluated for the different aeration-agitation systems used. The average absolute error (AAE) and average relative error (ARE) of estimation with each model, evaluated in the following ranges of the variables $250 \le P_g/V_L \le 850$ W/m^3; $1\ 10^{-3} \le \upsilon_G \le 5\ 10^{-3}$ m/s, are shown in Tab. 4. As can be observed, the average relative error of estimation in all the models is larger than 14 %, while the authors have reported an ARE of estimation of 8 % with their experimental data. The model proposed by Nocentini *et al.* [25] overestimates the k_La found in this work, while the rest of the models underestimate it.

Taking this situation into account, all the k_La experimental data was correlated as a function of the P_g/V_L and gas superficial velocity by using the model proposed by Cooper *et al.* [30].

$$k_La = c\left(\frac{P_g}{V_L}\right)^A (\upsilon_G)^B \qquad (3)$$

The model parameters A, B, and c, calculated by means of the least-squares method, were A = 0.48, B = 0.59 and c = 0.035, obtaining this way an AAE and ARE of 0.0022 s^{-1} and 11.9 %, respectively. As can be remarked, the model parameters provide an improvement of only 2 %, approximately, in the fit of the experimental data.

This situation suggests that in Cooper's k_La correlation, the model parameters depend on the impeller-sparger geometry [31]. This differs from the criterion that for a given value of power consumption per unit volume and superficial gas velocity, the same mass transfer rate can be achieved provided that the flow in the mixing vessel is fully turbulent and the gas bubbles are well dispersed [21,32,33].

As a matter of fact, the impeller-sparger geometry has a great influence on the mass transfer process because it determines the flow pattern of the air bubbles and, therefore, whether or not bubbles are dragged directly or indirectly by the flow streams toward the areas of maximum shear [2]. However, in the reviewed literature, no models appear to ex-

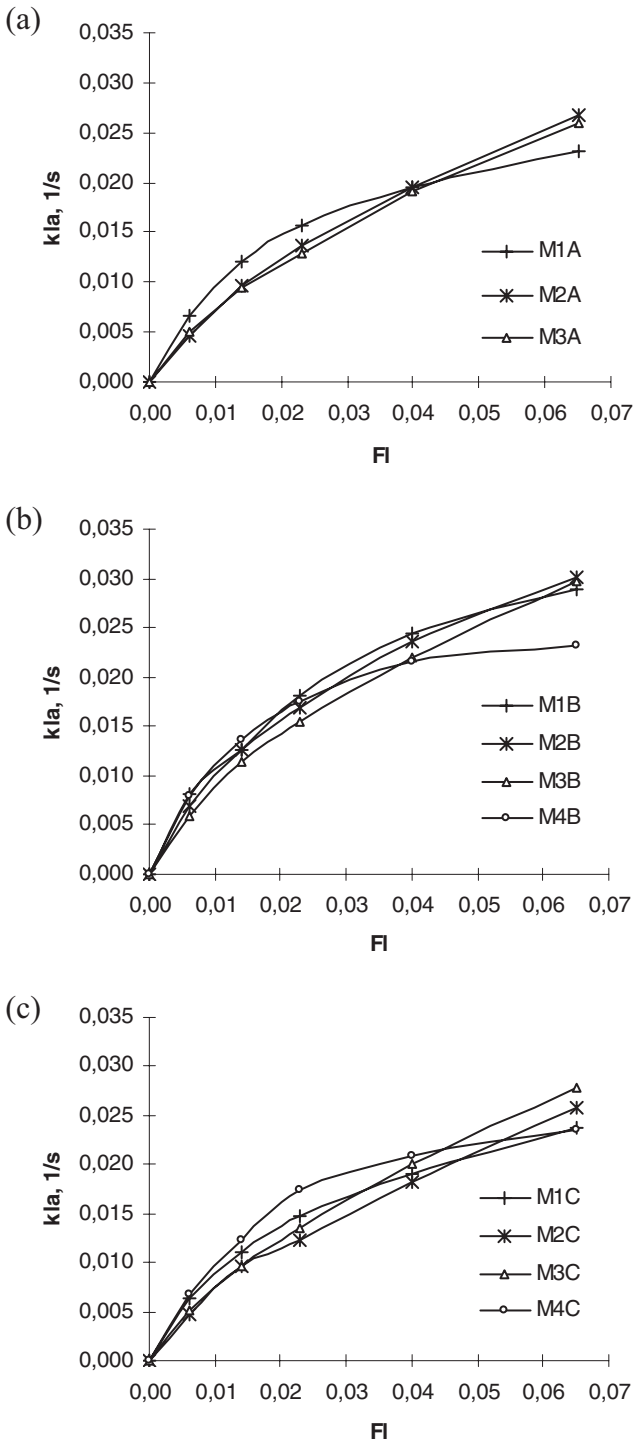

Figure 6. Overall mass transfer coefficient in the reactor arrangement with C = 0.33 T. a) single impeller, b) dual impellers of the same diameter and c) dual impellers of different diameters.

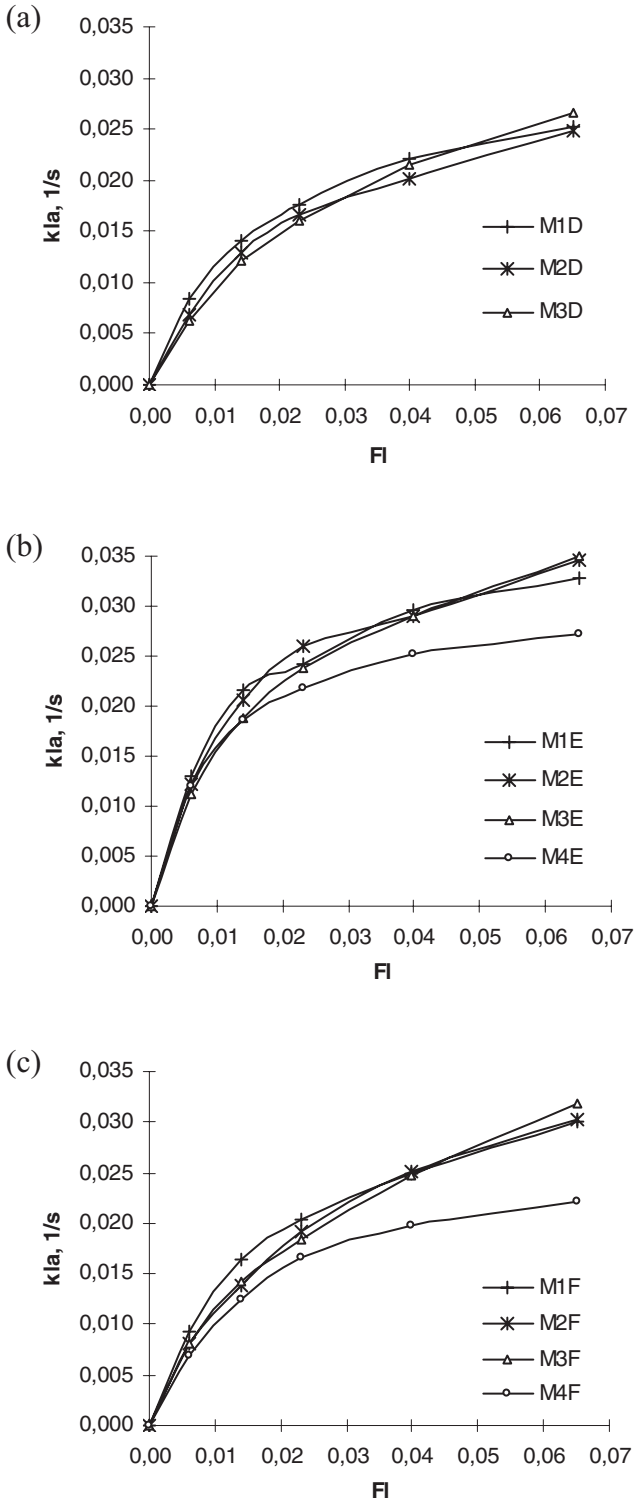

Figure 7. Overall mass transfer coefficient in the reactor arrangement with C = 0.25 T. a) single impeller, b) dual impellers of the same diameter and c) dual impellers of different diameters.

ist that take this influence into account. Besides, it was also verified that there are different opinions about which variable for the gas flow should be used in the correlations (superficial gas velocity or volumetric gas flow rate per unit volume) from the scaleup point of view. For example, Judat [22] correlating the k_La data set measured in reactors of different volumes found that only using the k_La as a function of the power per unit volume and the superficial gas velocity could correlate all the data in a curve, while Schlüter and Deckwer [24] verified experimentally the same phenome-

Table 4. k_La estimation errors with different models.

Reference	Models	AAE, s^{-1}	ARE, %
Smith [23]	$k_La = 0.000125\left(\frac{D}{T}\right)^{2.8} Fr^{0.6} Re^{0.7} Fl^{0.45} \left(\frac{D}{g}\right)^{-0.5}$	0.0031	14.4
Nocentini *et al.* [25]	$k_La = 0.015\left(\frac{P_g}{V_L}\right)^{0.59} v_G^{0.55}$	0.0025	14.2
Vasconcelos *et al.* [28]	$k_La = 0.0062\left(\frac{P_g}{V_L}\right)^{0.66} v_G^{0.51}$	0.0036	17.1
Linek *et al.* [29]	$k_La = 0.00495\left(\frac{P_g}{V_L}\right)^{0.593} v_G^{0.4}$	0.0038	17.9

non, but with the k_La as a function of the power per unit volume and the volumetric gas flow rate. Keeping these evidences in mind, it can be stated that more experimental data are necessary to elucidate which of the two approaches is more appropriate or in which case each variable should be used. On the other hand, Schlüter and Deckwer [24] stressed that if one does not consider any variations of the physicochemical properties and takes only the dependencies of k_La on the reactor operating conditions into account, the more recently proposed correlations all reduce to one of the two types, namely,

$$k_La \sim \left(\frac{P_g}{V_L}\right)^A (v_G)^B \tag{4}$$

$$k_La \sim \left(\frac{P_g}{V_L}\right)^A \left(\frac{Q_g}{V_L}\right)^B \tag{5}$$

In view of this fact, the experimental data have been correlated using both forms of the model that were modified by adding a coefficient which takes the impeller-sparger geometry into account. In the literature reviewed, no modification of Cooper's model similar to this has been reported.

$$k_La = c\left(\frac{P_g}{V_L}\right)^A (v_G)^B K \tag{6}$$

$$k_La = c\left(\frac{P_g}{V_L}\right)^A \left(\frac{Q_g}{V_L}\right)^B K \tag{7}$$

$$K = \exp\left(h\frac{C}{D_L} + f\frac{IC}{D_L} + g\frac{S_d}{D_L}\right) \tag{8}$$

The coefficients of the previous equations were determined by means of a nonlinear regression, minimizing the sum of the squares of the residuals by a Newton method. The correlations obtained reduce the average absolute error and the average relative error to 0.0015 s^{-1} and 8 %, respectively, in both cases. The parameters of the models are shown in Tab. 5. An example of the agreement between measurements and predictions using the model a) is presented in Fig. 8.

The significance of all the model coefficients was tested by an analysis of variance (a Fischer test) in which the variance of the residuals of the complete model was compared with the variance of the residuals of the submodels whereby one of the coefficients was suppressed with its respective variable. This way, it was verified that all the values of F_{cal} were greater than F_{tab} with a confidence level of 99 %.

3.3 Overall Transfer Efficiency

The overall oxygen transfer efficiency (OTE) corresponds to the energetic cost for transferring a given quantity of oxy-

Table 5. Fitted parameters of the correlation equations.

Model	A	B	c	h	f	g
a) $k_La = c\left(\frac{P_g}{V_L}\right)^A (v_G)^B K$	0.43	0.54	0.056	–0.50	0.07	–0.08
b) $k_La = c\left(\frac{P_g}{V_L}\right)^A \left(\frac{Q_g}{V_L}\right)^B K$	0.43	0.54	0.023	–0.50	0.07	–0.08

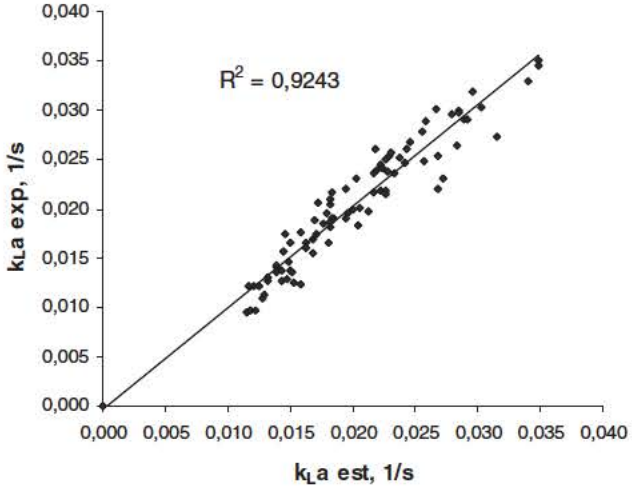

Figure 8. Correlation between experimental and predicted values of $k_L a$ by means of equation $k_L a = 0.056\left(\frac{P_g}{V_L}\right)^{0.48}(v_G)^{0.54} e^{\left(0.07\frac{IC}{D_L} - 0.5\frac{C}{D_L} - 0.08\frac{S_d}{D_L}\right)}$.

gen into the liquid phase. The OTE variation is shown as a function of flow number and sparger position in the systems with different impeller configurations in Fig. 9.

In Figs. 9a) and d) it is shown that in the single impeller configuration the small sparger located below the impeller is the most efficient. It is necessary to point out that although Birch and Ahmed [2] reported that in the single impeller configuration at C = 0.33 T the sparger located level with the impeller provides the higher gas holdup. This does not lead to the best oxygen transfer efficiency with the reactor geometry used in this work.

On the other hand, in Figs. 9b) and c) it can be observed that for weak values of the Fl the sparger configuration located between the impellers is the most efficient for the configurations with dual impellers located at C = 0.33 T. This phenomenon is more evident in the configuration with both impellers of different diameters.

In order to compare in a general way the different impeller configurations with regard to the OTE, the values of the OTE obtained with all the sparger configurations for each impeller configuration were averaged (see Fig. 10).

As can be noticed, the impeller configuration F with C = 0.25 T where the impellers have different diameters was the most effective for transferring oxygen through the gas/liquid interface per unit of power consumed.

In the same way, to determine the most efficient sparger configuration, the values of the OTE obtained with all the impeller configurations for each sparger configuration were averaged (see Fig. 11).

As can be observed in the figure, in general, the configuration with the sparger of smaller diameter located below the lower impeller was the most efficient among all the impeller configurations.

3.3.1 Overall Transfer Efficiency Modeling

Bouaifi and Roustan [10] proposed a model to estimate the OTE similar to the one used by Cooper *et al.* [30] to estimate the volumetric mass transfer coefficient:

$$OTE = c_1\left(\frac{P_g}{V_L}\right)^{A1}(v_G)^{B1} \tag{9}$$

Evaluating the prediction capacity of the model with our experimental data, an AAE and an ARE of 0.13 kgO_2/kWh and 15 % were obtained respectively. It is necessary to point out that the liquid height (H = 2 T) and the range of superficial gas velocity ($5.4\ 10^{-3} \le v_G \le 18\ 10^{-3}\ m.s^{-1}$) used by Bouaifi and Roustan [10] in their experiments were higher than those used in this study. The correlation of the experimental data with the model improved the fit an AAE of 0.10 $kgO_2/kW\ h$ and an ARE of 12 %. Taking this into account, the model was modified introducing a coefficient that considers the effect of the impeller-sparger geometry:

$$OTE = c_1 10^3\left(\frac{P_g}{V_L}\right)^{A1}(v_G)^{B1} K1 \tag{10}$$

where

$$K1 = \exp\left(h\frac{C}{D_L} + g\frac{S_d}{D_L}\right) \tag{11}$$

In this case, the AAE was 0.07 $kgO_2/kW\ h$ and the ARE 9 %. The determination of the coefficients and the analysis of the significance were done in the same way described previously for the $k_L a$ model. It is necessary to point out that from this analysis the coefficient of the parameter IC/D_L is not significant. The coefficients of the two models are shown in Tab. 6. The agreement between the experimental and calculated data is presented in Fig. 12.

4 Conclusions

The impeller configuration with an upper turbine smaller than the lower one could have a practical use due to the better distribution of the power drawn in the bulk reactor volume, without a dramatic increase in the power demand.

Experimental results show that the greatest values of the overall mass transfer coefficient in the different impeller configurations studied were obtained at low gas flow rates for the sparger with the ring diameter smaller than the impeller diameter and positioned below the impeller. An exception was the impeller configuration with impeller of different diameters located at C = IC = 0.33, for which the arrangement of the smaller sparger located between the impellers was the best one. On the other hand, it was stated that at higher gas flow rates the biggest values of $k_L a$ are obtained with the spargers of large ring diameter.

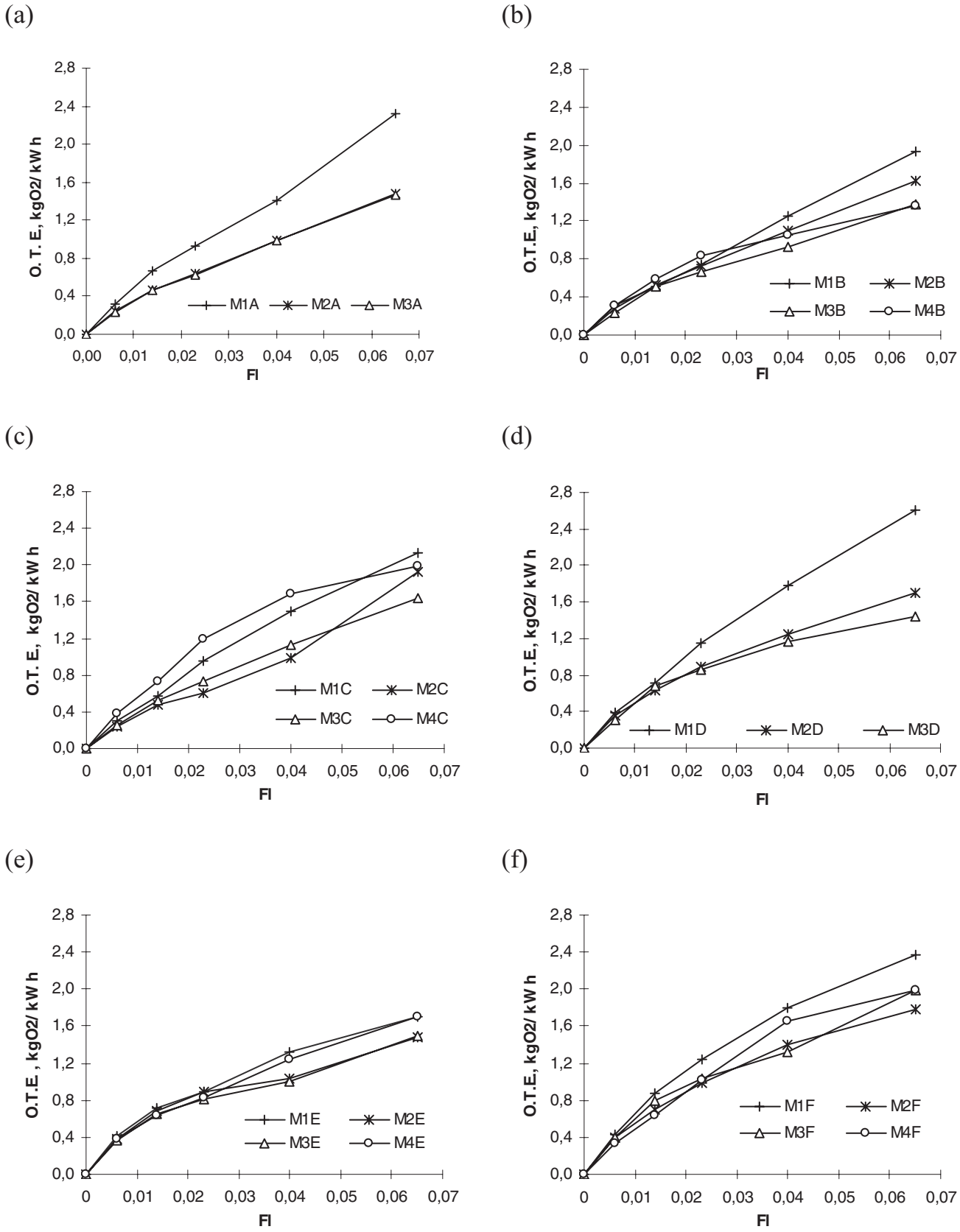

Figure 9. OTE with the following impeller configurations: with C = 0.33 T (a) single impeller, b) dual impellers of the same diameter and c) dual impellers of different diameters) and with C = 0.25 T (d) single impeller, e) dual impellers of the same diameter and f) dual impellers of different diameters).

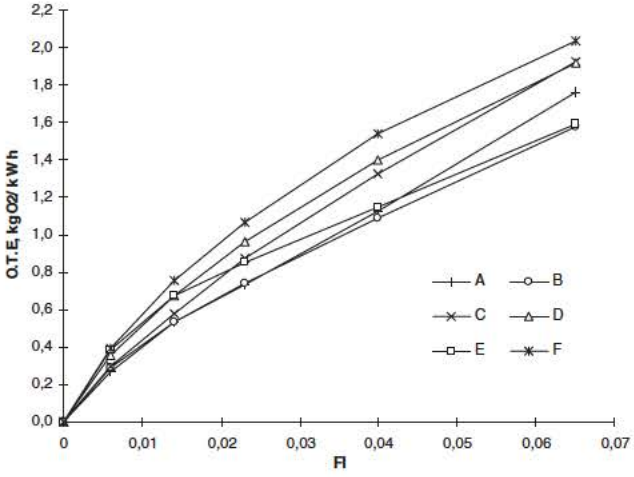

Figure 10. OTE averaged in regard to sparger configurations for each impeller configuration.

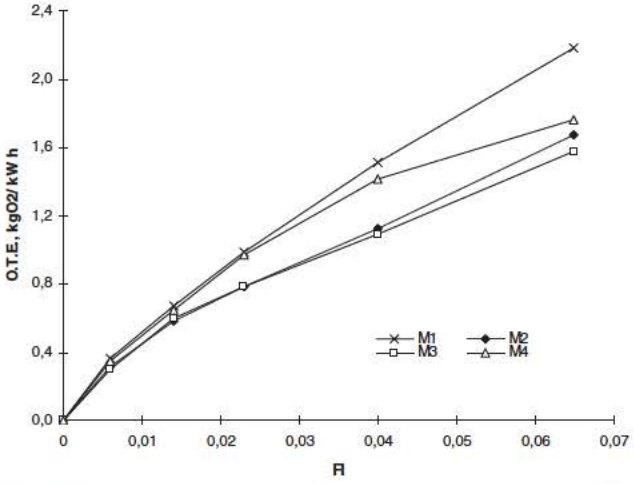

Figure 11. Overall oxygen transfer efficiency averaged in regard to impeller configurations for each sparger configuration.

Two new models to estimate the k_La and the overall oxygen transfer efficiency were proposed, which take the reactor operating conditions and the influence of the impeller-sparger geometry into account. The models allow to estimate the k_La and the overall oxygen transfer efficiency with an average relative error of 8 and 9 %, respectively.

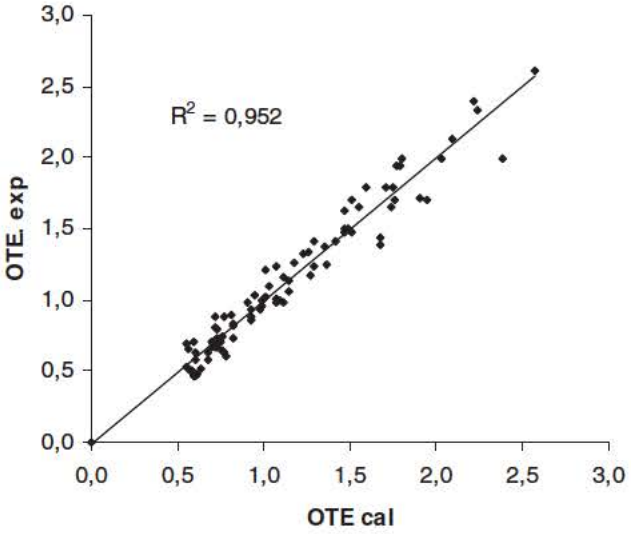

Figure 12. Correlation between experimental and predicted values of OTE by means of equation $OTE = 1.57\times10^{3}\left(\frac{P_g}{V_L}\right)^{-0.55}(v_G)^{0.56}e^{-\left(0.1\frac{C}{D_L}+0.4\frac{S_1}{D_L}\right)}$.

The results show that, in the studied range of gas flow rates, the most efficient impeller-sparger arrangement for the oxygen transfer is the impeller system with turbines of different diameters located at C = 0.25 and IC = 0.5 with the small diameter sparger settled below the lower impeller. Other arrangements could have other interesting capabilities, for example, a larger capacity of gas dispersion, which could allow to work at higher gas flow rates without flooding. This point will be verified in further work.

Acknowledgements

DGC would like to acknowledge ALFA program project for the award of the fellowship that made this work possible.

Received: October 27, 2003 [CET 1965]

Symbols used

A, A1, B, B1, f, g, h	[ ]	model exponents, dimensionless

Table 6. Fitted parameters of the correlation equations.

Model	A1	B1	c_1	h	g
a) $OTE = c_1\left(\frac{P_g}{V_L}\right)^{A1}(v_G)^{B1}$	Coefficients obtained by Bouaifi and Roustan [10]				
	–0.50	0.60	773	–	–
	Coefficients obtained in this study				
	–0.54	0.54	798	–	–
b) $OTE = c_1 10^3\left(\frac{P_g}{V_L}\right)^{A1}(v_G)^{B1}K1$	–0.55	0.56	1.57	–0.10	–0.46

C	[m]	clearance of the impeller from the tank bottom
C*	[kg m^{-3}]	equilibrium concentration of the oxygen dissolved in water
c, c_1, K, K1	[ ]	model coefficients, dimensionless
C_{gi}	[kg m^{-3}]	oxygen concentration in the feeding gas
C_L	[kg m^{-3}]	oxygen concentration in the liquid phase
C_{Lm}	[kg m^{-3}]	oxygen concentration measured experimentally with the oxygen probe
D	[m]	impeller diameter
F_{cal}	[ ]	calculated Fisher criterion, dimensionless
F_{tab}	[ ]	tabulated Fisher criterion, dimensionless
Fl	[ ]	flow number = Qg/ND^3, dimensionless
H	[m]	fluid height
IC	[m]	clearance between impellers
k_La	[s^{-1}]	volumetric mass transfer coefficient
m	[ ]	partition coefficient, dimensionless
N_p	[ ]	impeller power number, dimensionless
P_g, P	[W]	power consumption under gassed conditions
P_o	[W]	ungassed power consumption
Q_g	[m^3 s^{-1}]	volumetric gas flow rate
r	[m]	bottom curvature radius
Re	[ ]	Reynolds number = $\rho ND^2/\mu$, dimensionless
S	[m]	clearance from the lower impeller to the sparger
S_d	[m]	sparger diameter
t	[s]	time
T	[m]	inner vessel diameter
V_L	[m^3]	liquid volume in the vessel
z	[m]	height from the reactor bottom

Greek letters

τ	[s]	response lag of the oxygen probe
υ_G	[m s^{-1}]	superficial gas velocity
ρ	[kg m^{-3}]	density

Subscripts

1,2	single or two impellers, respectively
L	lower

Abbreviations

AAE	average absolute error
ARE	average relative error
OTE	overall transfer efficiency

References

[1] J. M. Smith, in *Mixing of Liquids by Mechanical Agitation* (Eds: J. J. Ulbrecht, G. K. Patterson), Gordon and Breach Science Publishers, New York **1985**.
[2] D. Birch, N. Ahmed, *Chem. Eng. Res. Des.* **1997,** *75(A5)*, 487.
[3] J. A. Rocha-Valadez, E. Galindo, L. Serrano-Carreón, *Bioproc. Eng.* **2000**, *23,* 403.
[4] A. W. Nienow, L. Huoxin, W. Haozhung, K. V. Allsford, D. Cronin, V. Hudcova, in *Proc. of the 2nd Int. Conf. on Bioreactor Fluid Dynamics*, Cambridge, UK, Sep. 21–23, **1988**, 159.
[5] V. Abrardi, G. Rovero, S. Sicardi, G. Baldi, R. Conti, in *Proc. of the 6th Eur. Conf. on Mixing*, Pavia, Italy, BHRA Fluid Eng., Cranfield, England **1988,** 329.
[6] V. Hudcova, V. Machon, A. W. Nienow, *Biotech. Bioeng.* **1989,** *34*, 617.
[7] R.-V. Roman, M. Gavrilescu,. *Hung. J. Ind. Chem. Vesz.* **1994,** *22*, 87.
[8] J. M. T. Vasconcelos, S. Alves, A. W. Nienow, W. Bujalski,. *Can. J. Chem. Eng.* **1998,** *76*, 399.
[9] R. Kuboi, A. W. Nienow, in *Proc.of the 4th Eur. Conf. on Mixing*, Noordwijkerhout, The Netherlands, April 27–29, **1982,** 247.
[10] M. Bouaifi, M. Roustan, *Can. J. Chem. Eng.* **1998**, *76(3)*, 390.
[11] K. Rutherford, K. C. Lee, S. M. S. Mahmoudi, M. Yianneskis, *AIChE J.* **1996**, *42(2)*, 332.
[12] V. Machon, J. Vlcek, V. Hudcová, in *Proc. of the 6th Eur. Conf. on Mixing*, Pavia, Italy, BHRA Fluid Eng, Cranfield, England, **1988**, 351.
[13] V. Linek, P. Beneš, F. Hovorka, *Biotech. Bioeng.* **1981**, *23*, 301.
[14] M. M. Lopes de Figueiredo, P. H. Calderbank, *Chem. Eng. Sci.* **1979**, *34*, 1333.
[15] A. Bakker, Hydrodynamics of Stirred Gas-Liquid Dispersions, *Ph.D. Thesis*, Delft University of Technology, The Netherlands, **1992**.
[16] B. Atkinson, F. Mavituna, *Biochemical Engineering and Biotechnology Handbook*, 2nd ed., M. Stockton Press, New York **1999**.
[17] V. Schlüter, W. D. Deckwer, in *Proc. of the 3rd Int. Conf. on Bioreactor and Bioprocess Fluid Dynamics*, Cambridge, UK, **1993**, 117.
[18] V. Abrardi, G. Rovero, G. Baldi, S. Sicardi, R. Conti, *Chem. Eng. Res. Des.* **1990**, *68*, 516.
[19] F. Chiampo, R. Guglielmetti, L. Manna, R. Conti, in *Proc. of the 7th Eur. Conf. on Mixing*, Bruges, Belgium, Sep. 18–20, **1991**, 333.
[20] A. W. Nienow, M. M. C. G. Warmoeskerken, J. M. Smith, M. Kono, in *Proc. of the 5th Eur. Mixing Conf.*, Germany; BHRA Fluid Engineering, Cranfield, **1985**, 143.
[21] K. Van't Riet, *Ind. Eng. Chem. Proc. Des. Dev.* **1979**, *18(3)*, 357.
[22] H. Judat, *Ger. Chem. Eng.* **1982**, *5*, 357.
[23] J. M. Smith, in *Proc. of the 7th Eur. Conf on Mixing*, Bruges, Belgium, Royal Flemish Society of Engineers, Belgium, Part I, **1991**, 233.
[24] V. Schlüter, W. D. Deckwer, in *Proc. of the 3rd Int. Conf. on Bioreactor and Bioprocess Fluid Dynamics*, Cambridge, UK, **1993**, 117.
[25] M. Nocentini, D. Fajner, G. Pasquali, F. Magelli, *Ind. Eng. Chem. Res.* **1993**, *32*, 19.
[26] V. Linek, T. Moucha, J. Sinkule, *Chem. Eng. Sci.* **1996**, *51(12)*, 3203.
[27] H. Wu, V. Arcella, M. A. Malavasi, *Chem. Eng. Sci.* **1998**, *53(5)*, 1089.
[28] J. M. T. Vasconcelos, S. C. P. Orvalho, A. M. A.- F. Rodriguez, S. S. Alves, *Ind. Eng. Chem. Res.* **2000**, *39(1)*, 203.
[29] V. Linek, V. Vacek, P. Beneš, *Chem. Eng. J.* **1987**, *34*, 11.
[30] C. M. Cooper, G. A. Fernstrom, S. A. Miller, *Ind. Eng. Chem.* **1944**, *36*, 504.
[31] M. Moresi, M. Patete, *J. Chem. Tech. Biotechnol.* **1988**, *42*, 197.
[32] Z. D. Chen, J. J. Chen, *Chem. Eng. Res. Des.* **1999**, *77*, 104.
[33] Y. Zhu, P. C. Banddopadhayay, J. Wu, *3rd Int. Symp. on Mixing in Industrial Processes*, Japan, **1999**, 389.